Charge ordering and low-temperature lattice distortion in the β^{′}-(BEDT-TTF)_{2}CF_{3}CF_{2}SO_{3} dimer Mott insulator

I. Olejniczak, R. Wesołowski, H. O. Jeschke, R. Valentí, B. Barszcz, and J. A. Schlueter

Phys. Rev. B **101**, 035150 — Published 29 January 2020

DOI: 10.1103/PhysRevB.101.035150

Charge Ordering and Low Temperature Lattice Distortion in the β'-(BEDT-TTF)$_2$CF$_3$CF$_2$SO$_3$ Dimer Mott Insulator

I. Olejniczak,[1] R. Wesołowski,[1] H.O. Jeschke,[2] R. Valentí,[3] B. Barszcz,[1] and J.A. Schlueter[4,5]

[1] *Institute of Molecular Physics, Polish Academy of Sciences, Smoluchowskiego 17, 60-179 Poznań, Poland*
[2] *Research Institute for Interdisciplinary Science, Okayama University, Okayama 700-8530, Japan*
[3] *Goethe-Universität Frankfurt, Institut für Theoretische Physik, Max-von-Laue-Straße 1, 60438 Frankfurt am Main, Germany*
[4] *Materials Science Division, Argonne National Laboratory, Argonne, IL 60439, USA*
[5] *Division of Materials Research, National Science Foundation, 2415 Eisenhower Avenue, Alexandria, VA 22314, USA*

We present single-crystal X-ray diffraction measurements, optical investigations and electronic structure calculations for the organic charge-transfer salt β'-(BEDT-TTF)$_2$CF$_3$CF$_2$SO$_3$ synthesized by electrocrystallization. Electronic structure calculations confirm the quasi-one-dimensional behavior of the compound and optical conductivity measurements reveal the dimer-Mott insulating nature of the system. The splitting of the charge-sensitive ν_2 mode in Raman spectra demonstrates the onset of an interlayer charge-ordered phase below 25 K, also suggested by the crystal structure considerations. This transition is accompanied by clear signatures of a lattice distortion in the BEDT-TTF donor layer, as shown by a splitting of the vibrational ν_3 mode in infrared spectra. At the same time, the sharp redshift of the ν_1 mode involving the BEDT-TTF ethylene groups strongly suggests a significant modification of the hydrogen-type bonding present between the BEDT-TTF donor layer and the $CF_3CF_2SO_3^-$ anion layer. These observations point to a subtle interplay of charge and lattice degrees of freedom at the phase transition.

INTRODUCTION

The (BEDT-TTF)$_2X$ organic charge transfer salts, where BEDT-TTF is bis(ethylenedithio)tetrathiafulvalene and X^- is a monovalent charge-compensating anion, have attracted considerable interest due to a variety of phases related to the correlated nature of the layer of BEDT-TTF molecules [1–7]. Depending on the geometrical arrangement (motif) of the BEDT-TTF molecules, these systems form different quasi-two dimensional and quasi-one dimensional structural families denoted as α, β, β', β'', or κ phases [1, 4], and exhibit rich phase diagrams including antiferromagnetic Mott insulating, dimer-Mott insulating, charge-ordered, superconducting, and spin-liquid phases [1, 4, 8–10].

Charge ordering (CO) manifests as ordered charge accumulation/depletion in the BEDT-TTF donor layer and originates from a competition between BEDT-TTF intramolecular and intermolecular Coulomb repulsion. Recently, special attention has been devoted to CO in the κ-(BEDT-TTF)$_2$X family and to its possible relation to electronic ferroelectricity and structural fluctuations [11, 12]. Motivated by these findings, we focus our attention on the possibility of the appearance of such phases in (BEDT-TTF)$_2$X with a different lattice motif. In the present work, we present a detailed study of the electronic and structural properties of β'-(BEDT-TTF)$_2$CF$_3$CF$_2$SO$_3$ by a combination of single-crystal X-ray diffraction measurements, optical investigations and *ab initio*-based electronic structure calculations.

In the family (BEDT-TTF)$_2$SF$_5R$SO$_3$, where R = CH_2, CF_2, CHF, $CHFCF_2$, CH_2CF_2, structural as well as electronic properties of the resulting material strongly depend on the anion which can be easily modified prior to the crystallization process [13, 14]. β''-(BEDT-TTF)$_2$SF$_5$CH$_2$CF$_2$SO$_3$ has been discussed as a model compound for superconductivity mediated by CO fluctuations [15–18]. In the case of β'-(BEDT-TTF)$_2$SF$_5$CF$_2$SO$_3$, where the β' packing motif is characterized by a dimerized one-dimensional stacking of the BEDT-TTF molecules, early electron spin resonance (ESR) experiments revealed a spin gap at about 30 K [19] and a vibrational study indicated a weak lattice distortion at the same temperature [20]. Both results were regarded as consistent with the spin-Peierls mechanism. Later high-field ESR and nuclear magnetic resonance (NMR) experiments rather suggested the onset of antiferromagnetic correlations at low temperatures [21]. In the present work we concentrate on β'-(BEDT-TTF)$_2$CF$_3$CF$_2$SO$_3$ [22] and explore the effect of exchanging the SF_5 group with CF_3 in the anion. Examining the crystal and electronic structure as well as the optical properties, we confirm the dimer Mott insulating nature of the system and find a transition at $\approx$ 20 K to an interlayer charge-ordered phase, accompanied by a significant lattice distortion that influences the molecular interactions between donor and anion layers.

SYNTHESIS, EXPERIMENTAL AND THEORETICAL METHODS

BEDT-TTF was prepared as described in Ref. [23, 24] and recrystallized from chloroform (Aldrich). Prior to use, 1,1,2-trichloroethane (TCE, Fluka) was dis-

tilled from phosphorus pentoxide (Aldrich) and filtered through a column containing neutral alumina. Tetrahydrofuran (THF, Aldrich) was distilled from sodium/benzophenone. 12-crown-4 (Acros) was used without further purification. Lithium pentafluoroethanesulfonate, Li($CF_3CF_2SO_3$), was prepared as described in Ref. [25]. PPN($CF_3CF_2SO_3$) [PPN^+ = bis(triphenylphosphoranylidene)ammonium] was prepared through a metathesis reaction of (PPN)Cl with Li($CF_3CF_2SO_3$). (PPN)Cl (Aldrich, 5.57 g, 9.71 mmol) was dissolved in 950 ml of water. Separately, Li($CF_3CF_2SO_3$) (2.0 g, 9.71 mmol) was dissolved in 50 ml. The two solutions were combined with the precipitation of PPN($CF_3CF_2SO_3$) as a white powder. This solid was recrystallized from acetone/diethyl ether, resulting in a white crystalline solid. Anal. Calcd for $C_{38}H_{30}P_2N_1S_1O_3F_5$: C, 61.87; H, 4.10; N, 1.90. Found: C, 61.59; H, 3.99; N, 1.86. Mp. 176-178 °C. Plate-like crystals of β'-(BEDT-TTF)$_2CF_3CF_2SO_3$ were grown through the use of the previously described electrocrystallization techniques,[14, 26, 27] as a minority phase in the following procedure. Li($CF_3CF_2SO_3$) (60 mg) and 12-crown-4 (10 mg) were added to 15 ml TCE and stirred for several minutes. This solution was divided between the two chambers of an H-cell. BEDT-TTF (10 mg) was loaded into the anode chamber. A current density of 0.10 μA/cm^2 was initially applied and gradually increased over a period of one week to 0.25 μA/cm^2, at which time crystallization of black crystals commenced on the electrode surface. Crystals were grown at 25 °C on platinum wire electrodes for a period of 27 days. Alternatively, PPN($CF_3CF_2SO_3$) (156 mg) was used as the electrolyte, replacing Li($CF_3CF_2SO_3$) and 12-crown-4.

High quality crystals were glued to the tip of glass fiber and mounted on a Bruker 3-circle diffractometer equipped with an APEX II detector. Data were collected at 300(2) K and 100(2) K, with temperature control achieved through use of an Oxford Cryostream 700 Plus LT Device. The data collection was carried out using MoKα radiation (λ = 0.71073 Å) with a frame exposure time of 30 seconds. The raw intensity data were corrected for absorption (SADABS [28]). The structure was solved and refined using SHELXTL.[29] A direct-method solution was calculated, which provided most of atomic positions from the electron density map. Full-matrix least squares / difference Fourier cycles were performed, which located the remaining atoms. All non-hydrogen atoms were refined with anisotropic displacement parameters. Hydrogen atoms were placed in ideal positions and refined as riding atoms with relative isotropic displacement parameters. Structural and refinement parameters are provided in Table I. Five hemispheres of data were collected with 0.30° ω scans and a detector distance of 60 mm. Data to a resolution of 0.77 Å were considered in the reduction, using a plate-like crystal of dimensions 0.50 x 0.10 x 0.02 mm^3.

Table I.
Crystal data and structure refinement of β'-(BEDT-TTF)$_2CF_3CF_2SO_3$.

Formula	$C_{22}H_{16}F_5O_3S_{17}$	
M_W	968.37	
Phase	β'	
Morphology	plate	
Cryst syst	triclinic	
Space group	$P\bar{1}$	
a/Å	6.6055(2)	6.5869(4)
b/Å	7.7518(3)	7.5224(5)
c/Å	34.7636(11)	34.710(2)
α/°	89.4390(10)	89.592(2)
β/°	88.7030(10)	87.526(2)
γ/°	74.2130(10)	73.440(2)
V/Å°	1712.46(10)	1646.98(18)
Z	2	
D_c/g cm^3	1.878	1.953
μ/mm^{-1}	1.128	1.173
$F(000)$	978	
R(int)	0.0309	0.0482
Total reflns	26031	24129
Unique reflns	7819	7439
$I > 2\sigma(I)$	6263	6836
$R(F_0), R_W(F_0^2)^a$	0.0764, 0.1986	0.1087, 0.2269
T/K	300(2)	100(2)

$^a R(F_0) = \sum \|\|F_0\| - \|F_c\|\| / \sum |F_0|, R_W(F_0^2) = [\sum w(|F_0^2| - |F_c^2|)^2 / \sum wF_0^2]^{1/2}$

We determined the electronic structure of β'-(BEDT-TTF)$_2CF_3CF_2SO_3$ by performing density functional theory calculations with the full potential local orbital (FPLO) basis [30] and using the generalized gradient approximation functional in its Perdew-Burke-Ernzerhof (PBE) form [31]. We employed projective Wannier functions within FPLO [32] to determine the tight binding Hamiltonian for the band arising from the HOMO level of BEDT-TTF. Calculations were performed on both the room temperature and 100 K crystal structures of β'-(BEDT-TTF)$_2CF_3CF_2SO_3$ reported in this paper. As described below, the T = 300 K structure has some disorder in the orientation of the pentafluoroethylsulfonate anions and in one ethylene endgroup of the BEDT-TTF molecules. We simplified the T = 300 K structure by choosing only the majority orientations.

For infrared measurements, a 2.2 × 0.7 × 0.1 mm^3 single crystal of β'-(BEDT-TTF)$_2SF_5CF_2SO_3$ was used. The optical axes of the crystal were determined as those displaying the largest anisotropy at 300 K. Two directions within the conducting plane were probed; one is close to the more conductive **b-a** direction and the other is close to the perpendicular **b+a** direction. Polarized infrared reflectance measurements in the frequency

range 600 - 7000 cm^{-1} were performed using a Perkin-Elmer 1725 X Fourier-transform infrared spectrometer, equipped with an Olympus infrared microscope, and a gold grid polarizer. For each polarization, reflectance spectra were measured at several temperatures between 10 and 300 K, and the temperature was controlled with an Oxford Instruments continuous-flow cryostat. In other frequency ranges, the 300 K polarized reflectance spectra were measured using a Perkin-Elmer Lambda 19 spectrometer (7000 - 30000 cm^{-1}), a Bruker Equinox 55 FT-IR spectrometer equipped with a Bruker IRScope II infrared microscope (7000 - 15000 cm^{-1}), and a Bruker 113V spectrometer with bolometer detector (50 - 600 cm^{-1}). The optical conductivity $\sigma_1(\omega)$ was calculated through the use of Kramers-Kronig analysis of the measured reflectance. First, we extended the range of data outside the middle infrared using 300 K spectra for all the temperatures. Then, the high-frequency data were extrapolated as ω^{-2}, and the low-frequency data were extrapolated as a constant, appropriate for semiconducting materials.[33] Optical conductivity spectra for $T = 300$ and 10 K have already been published in Ref. 34 and are reproduced here for comprehensive discussion. Raman spectra down to 10 K were recorded through the use of a Raman LABRAM HR800 spectrometer equipped with a microscope, a He-Ne 632.8 nm laser line (spectral resolution 2 cm^{-1}), and the Oxford Instruments continuous-flow cryostat; the spectra were collected in two separate experiments. The decomposition of the complex electronic and vibrational bands was performed by standard peak fitting techniques which allowed extraction of the center peak frequency and integral area (oscillator strength). Oscillators were fitted using a Voigt function which gave the most satisfactory results. Errors (standard deviations) were estimated statistically based upon the results obtained from slightly different ranges of data and/or baselines.

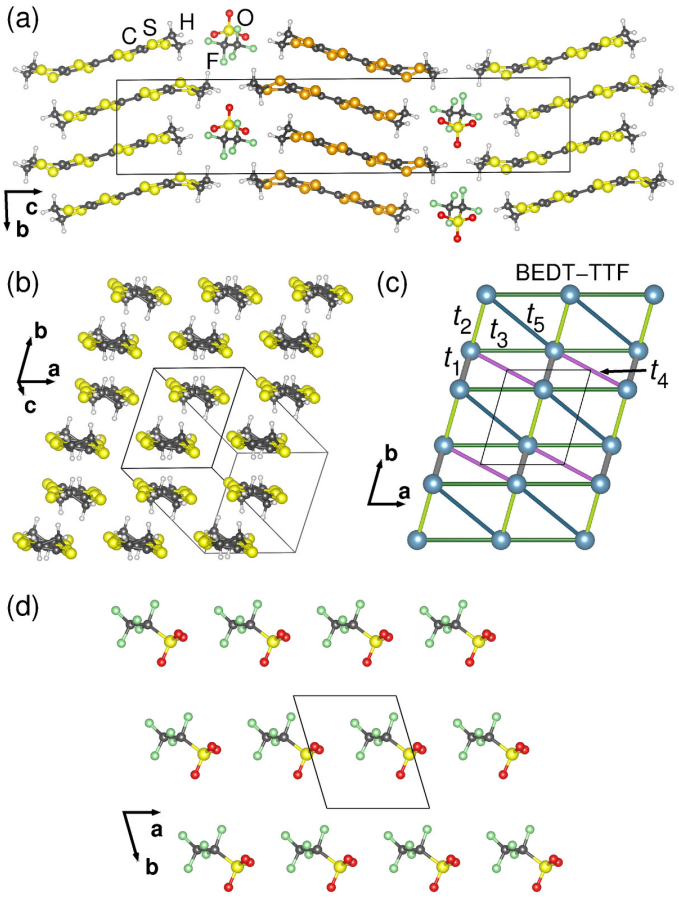

Figure 1. Packing diagrams of β'-(BEDT-TTF)$_2$CF$_3$CF$_2$SO$_3$ at 100 K. (a) BEDT-TTF molecules A and B are drawn with yellow and orange sulfur atoms, respectively. (b) BEDT-TTF layer of molecules A located at $z = 0$. (c) Lattice of BEDT-TTF molecule centers for β'-(BEDT-TTF)$_2$CF$_3$CF$_2$SO$_3$ with important hopping paths. (d) CF$_3$CF$_2$SO$_3^-$ anions.

RESULTS

Crystal Structure

β'-(BEDT-TTF)$_2$CF$_3$CF$_2$SO$_3$ crystallizes in the triclinic space group $P\bar{1}$ (see Table I). The structure is characterized by layers of partially oxidized BEDT-TTF molecules separated by anionic layers. There are two crystallographically nonequivalent BEDT-TTF molecules (hereafter designated as molecules A and B) per unit cell. As illustrated in Figure 1 (a), layers of BEDT-TTF molecules of type A are located at $z = 0$, while those of type B are located at $z = 0.5$. Both of these layers are characterized by dimerized stacking of BEDT-TTF molecules typical of the β' packing type.[35–37] Other structures with two equivalent conducting layers in the unit cell are observed in β'-Cat[Pd(dmit)$_2$]$_2$ salts, where Cat is a nonmagnetic monovalent cation such as Et$_2$Me$_2$P$^+$, EtMe$_3$Sb$^+$, etc., that display a solid crossing column structure.[38]

At room temperature one of the two ethylene groups of molecule B is disordered, with 82% of the groups in the staggered conformation. At 100 K, there is no significant disorder in the cation layers with the ethylene groups of both molecules A and B in the staggered conformation. Short intermolecular S$\cdots$S contacts, less than the 3.60 Å sum of van der Waals radii, are primarily present between BEDT-TTF molecules in adjacent stacks (Fig. 1 (b)). In the anionic layer located at $z = 0.75$, the R-SO$_3$ bonds in the anions point approximately along the **a**+**b** direction (Fig. 1 (d)), while in the layer located at $z = 0.25$, these bonds point along -(**a**+**b**).

It is useful to consider how seemingly minor changes in the anion structure result in significant modifications to the crystal structure. In the present case, the $R = SF_5$ group in β'-(BEDT-TTF)$_2$SF$_5$CF$_2$SO$_3$ has been replaced with a CF$_3$ group in the RCF$_2$SO$_3^-$ anion. Although

the BEDT-TTF radical cations in both the β'-(BEDT-TTF)$_2R$CF$_2$SO$_3$ (R = SF$_5$ or CF$_3$) structures pack in a β'-motif and have two crystallographically independent BEDT-TTF molecules, the overall structures are different. In the case of β'-(BEDT-TTF)$_2$CF$_3$CF$_2$SO$_3$, alternating *layers* have crystallographically unique molecules, while for β'-(BEDT-TTF)$_2$SF$_5$CF$_2$SO$_3$ each layer is identical, but there are alternating *stacks* within the layers (Supplemental Material,[39] Fig. S8). This is likely a result of the difference in packing within the anion layers: in the case of β'-(BEDT-TTF)$_2$CF$_3$CF$_2$SO$_3$ the dipole moments of the CF$_3$CF$_2$SO$_3^-$ anions within a layer all point in the same direction, while in the case of β'-(BEDT-TTF)$_2$SF$_5$CF$_2$SO$_3$, the SF$_5$CF$_2$SO$_3^-$ dipoles point in opposing directions in adjacent chains within the layers. For more structural details, see the Supplemental Material.[39]

Electronic Structure

Electronic band structures of β'-(BEDT-TTF)$_2$CF$_3$CF$_2$SO$_3$ are calculated for T = 100 K and room temperature within density functional theory with the PBE functional. Please note that the PBE functional incorrectly predicts a metallic state (see Supplemental Material [39]) and inclusion of correlation effects beyond the PBE functional in terms of a many-body approximation such as dynamical mean field theory are needed to describe the Mott insulating nature probed by the optical conductivity measurements. Such an approach has already been shown in the past to successfully describe the optical conductivity observations in other Mott insulating charge transfer salts [42]. Here we are primarily interested in the underlying network of hopping parameters of our system as well as in the distribution of molecular charges. This is well described with the PBE functional. The density of states that is resolved for the two symmetry inequivalent molecules in the two BEDT-TTF layers of the compound shows that there is a small charge disproportionation between the layers, i.e. a small charge difference between the BEDT-TTF molecules. Quantifying the charges by adding up the atom projected selfconsistent charges of the DFT run, we find charges of +0.44 and +0.42 at T = 100 K and of +0.46 and +0.43 at T = 300 K. Fig. 1 (c) shows the lattice of BEDT-TTF molecule centers, connected by the paths that turn out to have significant tight binding parameters. Tables II and III list the most important tight binding parameters. The largest values are t_1 and t_5 which leads to the predominantly one dimensional character of the material, with chains running in **b-a** direction (see Fig. 1 (c)). This is in good agreement with the Fermi surfaces that are corrugated sheets underlining the essentially one-dimensional nature of the compound (Fig. 2). Note that the importance of the t_5 hopping and thus the most conductive **b-a** direction can not be read off from either the dimer stacking direction (which is **b**) or the direction with the closest S-S contacts (which is **a**).

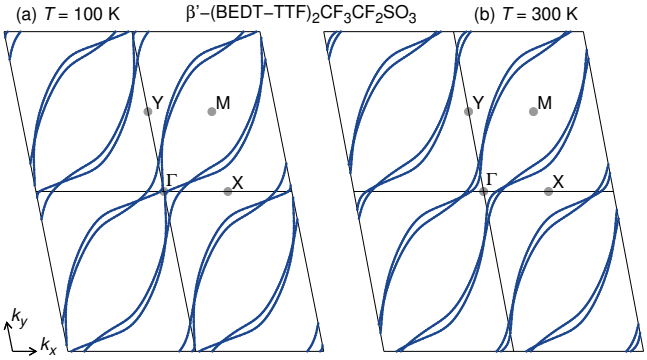

Figure 2. Fermi surface of β'-(BEDT-TTF)$_2$CF$_3$CF$_2$SO$_3$ at (a) T = 100 K and (b) T = 300 K.

	parameter	μ	t_1	t_2	t_3	t_4	t_5
ET(1)	distance (Å)	0	3.65	4.90	6.59	6.86	6.98
	value (meV)	-237.4	221.6	-73.0	-32.0	43.9	119.2
ET(2)	distance (Å)	0	3.72	4.92	6.59	6.78	7.11
	value (meV)	-246.3	205.6	-49.6	-21.9	55.4	123.8

Table II. Tight binding parameters of β'-(BEDT-TTF)$_2$CF$_3$CF$_2$SO$_3$ at T = 100 K (ET = BEDT-TTF); μ is the onsite energy/chemical potential. The strongest hopping t_1 is the hopping within the BEDT-TTF dimers, and the second strongest hopping t_5 along the **b-a** direction defines the most conductive in-plane direction.

	parameter	μ	t_1	t_2	t_3	t_4	t_5
ET(1)	distance (Å)	0	3.69	5.02	6.61	6.90	7.11
	value (meV)	-219.9	209.8	-53.2	-32.7	41.7	106.0
ET(2)	distance (Å)	0	3.73	5.01	6.61	6.83	7.20
	value (meV)	-235.6	204.7	-38.6	-22.3	48.7	103.3

Table III. Tight binding parameters of β'-(BEDT-TTF)$_2$CF$_3$CF$_2$SO$_3$ at T = 300 K (ET = BEDT-TTF); μ is the onsite energy/chemical potential.

Optical Properties: Dimer Mott Response

Figure 3 displays the infrared reflectance and optical conductivity spectra of β'-(BEDT-TTF)$_2$CF$_3$CF$_2$SO$_3$ polarized in the two principal polarization directions, measured at selected temperatures 300, 100 and 10 K. Substantially higher reflectance is detected in the **b-a** direction, which is a diagonal in the donor BEDT-TTF

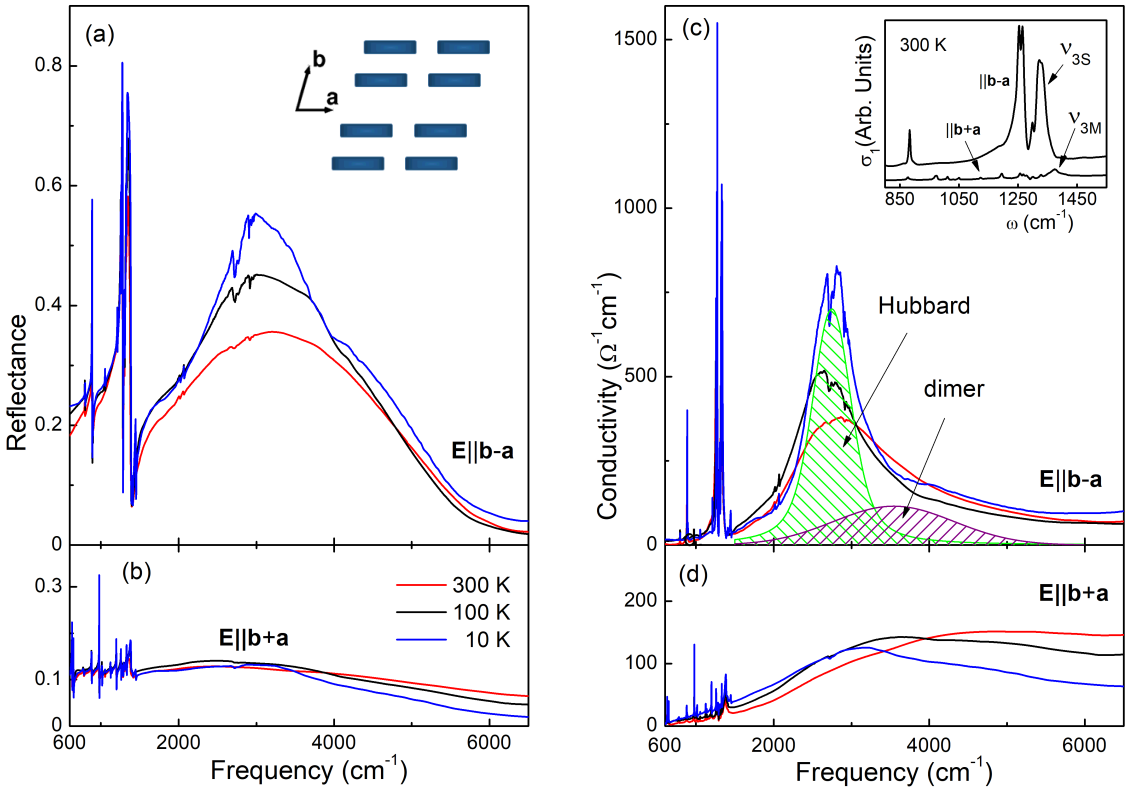

Figure 3. Polarized reflectance and optical conductivity spectra of β'-(BEDT-TTF)$_2$CF$_3$CF$_2$SO$_3$ for the **E**$\|$**b-a** (a, c) and **E**$\|$**b**+**a** (b, d) directions, at selected temperatures T = 300 K, 100 K and 10 K. The insets in panels (a) and (c) display the simplified structure of the conducting layer and a close-up view of the 300 K optical conductivity in the vibrational range, respectively. Two components, Hubbard and dimer, of the electronic band at 10 K, are marked in the panel (c).

plane (Fig. 3(a,b)). Such an anisotropic response is expected for a dimerized β'-type structure and in agreement with the results of band structure calculations that reveal a one-dimensional nature of the material (see Fig. 2) with strongest inter-dimer hopping along the **b-a** direction.

The overall shape of the spectra is characteristic for a dimer-Mott insulator, with a mid-infrared electronic band and relatively strong molecular vibrational modes below $\approx$ 1500 cm^{-1} (insets in Figs. 3(a,c)) that are known to originate from the coupling of the totally symmetrical modes of the BEDT-TTF molecule with the electronic transitions within the broken symmetry dimerized structure (electron-molecular vibration (e-mv) coupling).[43, 44] The optical conductivity spectra calculated based on the reflectance allow discussion of the low-lying electronic excitations that usually appear in the middle infrared frequency range due to the Coulomb interactions. At room temperature, the spectra of β'-(BEDT-TTF)$_2$CF$_3$CF$_2$SO$_3$ (Fig. 3(c,d)) display broad electronic absorption bands centered at about 2700 cm^{-1} and 4000 cm^{-1} in the **E**$\|$**b-a** and **E**$\|$**b**+**a** directions, respectively. The lowering of the temperature from 300 to 10 K mainly results in increased conductivity in the diagonal **b-a** direction in the relatively narrow range around the maximum of the asymmetric band at 2800 cm^{-1} (Fig. 3(c)). There is no change in the overall character of the spectra in both polarization directions.

Optical conductivity spectra of dimer-Mott insulators have been usually discussed within a dimerized picture at half-filling, that considers the interdimer and intradimer charge transfer (CT) as separate excitations.[42, 45] The interdimer CT (Hubbard band) is described in terms of a Hubbard model that takes into account the transitions between lower and upper Hubbard bands related with the effective on-dimer Coulomb interaction U. On the other hand, the intradimer excitation (dimer band) is assigned to a transition between bonding and antibonding orbitals of molecules in a dimer. In the strong dimerization limit (U, $V \ll t_1$, where t_1 is the intradimer transfer integral), the dimer band is expected to appear above

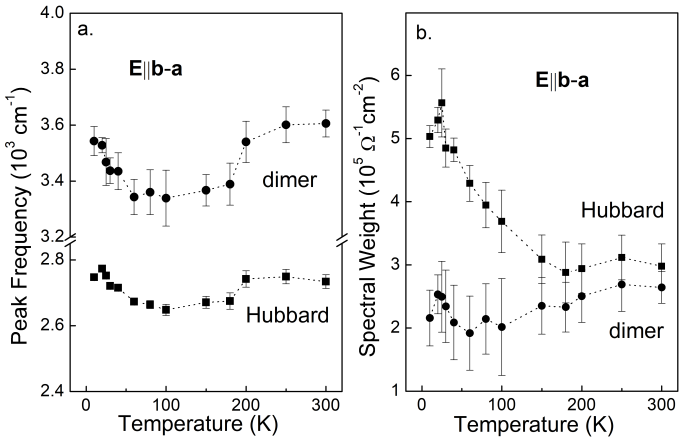

Figure 4. Temperature-dependent peak frequency (a) and oscillator strength (b) of two components of the mid-infrared band observed in the conductivity spectra of β'-(BEDT-TTF)$_2$CF$_3$CF$_2$SO$_3$ in the more conductive **b-a** direction, Hubbard band and dimer band.

the Hubbard band, at the frequency $\approx 2t_1$. Conductivity spectra of β'-(BEDT-TTF)$_2$CF$_3$CF$_2$SO$_3$ polarized in the more conductive **b-a** direction clearly show two components. Therefore we model the spectra using two oscillators, as shown for the 10 K spectrum in Fig. 3(c). Figure 4 presents the peak frequency (a) and oscillator strength (b) of these features as a function of temperature. At room temperature, the two bands are centered at ≈ 2700 cm^{-1} and 3600 cm^{-1} (Fig. 4(a)). The position of the higher frequency excitation shows excellent agreement with ≈ 3400 cm^{-1} (420 meV), the value estimated based on the electronic structure calculation with $2t_1$ (Table III). Therefore, we assign the 3600 cm^{-1} component to the dimer mode, and subsequently the lower frequency component that significantly increases its spectral weight (SW) on lowering the temperature (Fig. 4(b)) to the Hubbard band. Both electronic components slightly shift to lower frequency below 200 K on lowering the temperature, but this tendency is reversed below about 50 K (Fig. 4(a)).

The optical response of β'-(BEDT-TTF)$_2$CF$_3$CF$_2$SO$_3$ is similar to β'-(BEDT-TTF)$_2$SF$_5$CF$_2$SO$_3$,[20] as one could expect in view of the close chemical relationship between the two materials. Despite significant differences in the anion layer, we also notice close similarity with the dimer-Mott insulator β'-(BEDT-TTF)$_2$ICl$_2$.[46] Therefore, we can conclude that the overall ground state properties of β'-(BEDT-TTF)$_2$CF$_3$CF$_2$SO$_3$ are controlled by the degree of anisotropy of the lattice of dimers that constitute the conducting donor plane.

In the following discussion of optical properties of β'-(BEDT-TTF)$_2$CF$_3$CF$_2$SO$_3$ we focus on two issues: charge-ordering and low-temperature lattice distortion.

Raman Spectra: Charge-Order Transition

In order to explore the possibility of interlayer charge disproportionation suggested for β'-(BEDT-TTF)$_2$CF$_3$CF$_2$SO$_3$ by both the structural measurements and electronic structure calculations, we perform Raman scattering experiments in the frequency range of the C=C stretching vibrations that allow the estimation of charge on the donor molecules.[47] Assuming the planar D_{2h} point group symmetry for BEDT-TTF, these modes are labelled $\nu_2(A_g)$, assigned mainly to symmetric ring C=C stretching, bridge C=C stretching $\nu_3(A_g)$, and antisymmetric ring C=C stretching, $\nu_{27}(B_{1u})$. The modes ν_2 and ν_{27} are regarded as the best probes of the charge ρ localized on the donor molecule because these modes are only weakly affected or not affected by electron-molecular vibration coupling [47, 48].

Figure 5(a,b) displays the temperature dependence of the Raman spectra of β'-(BEDT-TTF)$_2$CF$_3$CF$_2$SO$_3$, polarized along the **b**+**a** direction. At room temperature, two bands observed centered at 1469 and 1492 cm^{-1} are assigned as ν_3 and ν_2, respectively, of the BEDT-TTF molecule with charge $+0.5e$. A weak shoulder at about 1460 cm^{-1} that develops into a separate band centered at 1464 cm^{-1} when lowering the temperature below 300 K, is most probably due to infrared-active ν_{27} activated in Raman as a result of the interaction within a symmetric dimer.[49] Such an interaction within a unit cell of the two modes of B_{1u} symmetry yields two modes, of which one is infrared-active and the other Raman-active.[50] Similar Raman spectra in this frequency range have been observed in the dimerized β'-(BEDT-TTF)$_2$ICl$_2$ salt.[51]

The peak positions of the ν_2, ν_3 and ν_{27} modes estimated based on a fitting analysis taking into account additional components for the ν_{27} and ν_2 modes below 30 K, are shown in Fig. 5(c). On lowering the temperature between 300 K and 30 K, ν_{27}, ν_3 and ν_2 gradually become narrower and slightly shift towards higher frequencies. Below 30 K a clear splitting of the ν_2 mode is observed (Fig. 5(a,b)). Such a behavior is usually discussed in terms of charge ordering. The charge disproportionation suggested in β'-(BEDT-TTF)$_2$CF$_3$CF$_2$SO$_3$ by the crystal structure measurements is far from the range where the hybridization between ν_2 and ν_3 could cause the deviation from the linear relationship $\nu_2(\rho) = 1447$ cm^{-1} + 120(1 - ρ) cm^{-1}, which is otherwise valid.[47] Therefore, we estimate the charge disproportionation $2\delta\rho$, from the frequency difference between the two ν_2 mode components, 1497 and 1509 cm^{-1} at 10 K, as $2\delta\rho \approx 0.1e$. While the observed ν_2 bands are slightly broadened due to the poor signal-to-noise level in the Raman experiment, there is no evidence for charge-order fluctuations in β'-(BEDT-TTF)$_2$CF$_3$CF$_2$SO$_3$ [52–54] and therefore we would conclude that the observed charge disproportionation corresponds to a charge ordered state.

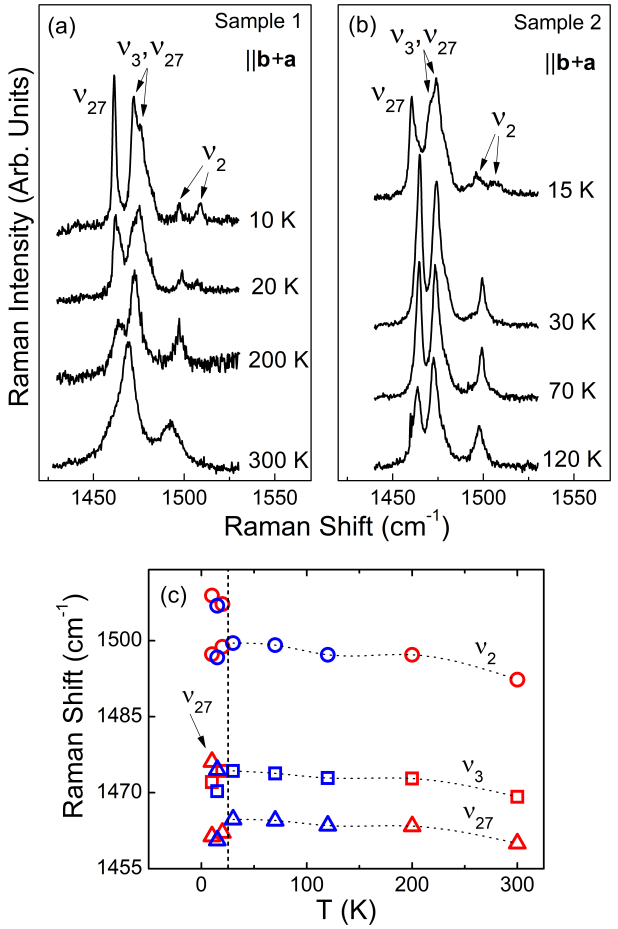

Figure 5. Temperature dependence of the Raman spectra of β'-(BEDT-TTF)$_2$CF$_3$CF$_2$SO$_3$ for Sample 1 (a) and Sample 2 (b). Polarization of the incident and detected light was parallel to the **b**+**a** direction; spectra are shifted for clarity. Panel (c) displays the Raman shift of the ν_{27} (Δ), ν_2 ($\bigcirc$), and ν_3 ($\square$) mode components, as observed in the spectra of Sample 1 (red color) and Sample 2 (blue). The dashed line marks the approximate temperature point below which the splitting of the ν_2 mode is observed. Lines between points are intended to guide the eye.

The ν_3 mode strongly couples to the electronic background and is therefore sensitive to structural modifications, including those related with charge order transition.[48, 55, 56] As a result the mode usually splits into several components that are infrared- and/or Raman-active. The highest frequency mode component is observed as a single band in Raman spectra where appears at the average frequency characteristic for the charge $0.5e$ even in the presence of charge disproportionation.[47, 56] In the Raman spectra of β'-(BEDT-TTF)$_2$CF$_3$CF$_2$SO$_3$, ν_3 appears as a single band between room temperature and $T \approx 30$ K. Upon cooling below this temperature, a significant change in the shape of the mode takes place that we interpret as the splitting of about 5 cm^{-1}. Taking into account the charge difference $2\delta\rho \approx 0.1e$ we suggest, that another component that appears at about 1476 cm^{-1} below 30 K is actually the charge sensitive ν_{27} mode (Fig. 5(c)). Similarly to ν_2, ν_{27} allows estimation of charge localized on the BEDT-TTF molecule, according to the formula $\nu_{27}(\rho) =$ 1398 cm^{-1} + 140(1 - ρ) cm^{-1}.[47] While at temperatures above 30 K, the observed frequency of the single ν_{27} mode corresponds to the charge of $\approx 0.5e$, on lowering below 30 K the mode component shifts to about 1461 cm^{-1} (Fig. 5(c)). If we consider the 1476 cm^{-1} band as another ν_{27} component, we can estimate the charge disproportionation from the frequency difference between 1461 and 1476 cm^{-1} at 10 K, as $2\delta\rho \approx 0.1e$, in agreement with the value estimated based on the ν_2 components.

Therefore, the Raman spectra provide a clear evidence that the observed charge disproportionation corresponds to charge ordering that appears in β'-(BEDT-TTF)$_2$CF$_3$CF$_2$SO$_3$ on lowering the temperature below 30 K. In order to give evidence for a lattice distortion associated with the charge ordering, we now focus on vibrational modes observed in infrared spectra.

Infrared Modes: Lattice Distortion

The ν_3 stretching C=C mode characterized by the large factor-group splitting is one of the most prominent vibrational features in the infrared spectra of low-dimensional organic conductors. The unit cell of β'-(BEDT-TTF)$_2$CF$_3$CF$_2$SO$_3$ accommodates four donor molecules involved in two conducting layers separated by anions, as shown in Fig. 1 (a). If these molecules are equivalent and do not interact, the ν_3 mode should be fourfold degenerate. On the other hand, in the presence of both a strong electron-molecular vibration interaction and charge ordering, as much as four different bands are expected in Raman and infrared spectra, depending on the crystal symmetry [47, 48, 55]. At room temperature, the conductivity spectra of β'-(BEDT-TTF)$_2$CF$_3$CF$_2$SO$_3$ reveal two modes in two different polarizations: the one marked ν_{3S} strongly perturbed by the e-mv interaction appears centered at 1327 cm^{-1} in the **b-a** direction, and the moderately perturbed ν_{3M} centered at 1374 cm^{-1} in the perpendicular direction (inset in Fig. 3(c)). No significant change is observed in the ν_3 mode down to about 25 K, where another ν_3 component, ν_{3H}, emerges centered at 1446 cm^{-1} in the conductivity spectra in both polarization directions (Fig. 6(a,b)). The strong temperature dependence of the mode (insets in Fig. 6) suggests, that a significant lattice distortion takes place in β'-(BEDT-TTF)$_2$CF$_3$CF$_2$SO$_3$ at about 25 K, most probably involving symmetry lowering. Taking into account another ν_3 component centered at about 1469 cm^{-1} in Raman spectra (Fig. 5(c)), we observe as much as four ν_3 modes at low T (Ta-

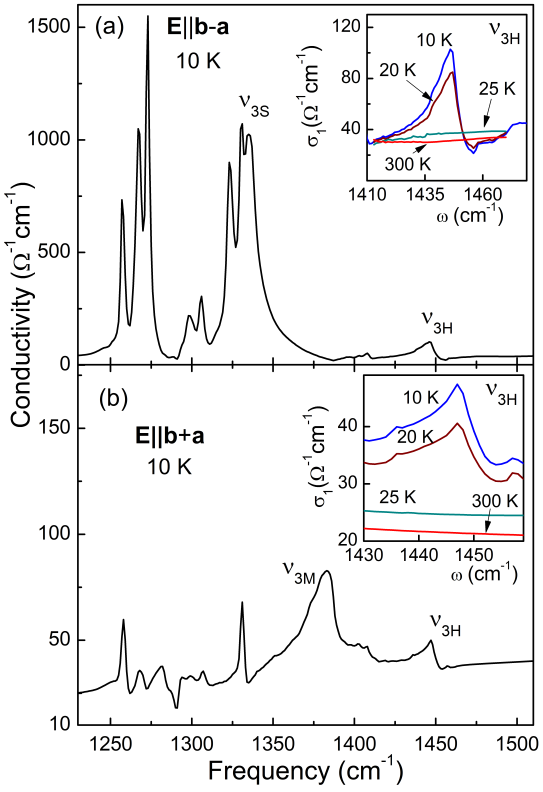

Figure 6. Optical conductivity spectra of β'-(BEDT-TTF)$_2$CF$_3$CF$_2$SO$_3$ at 10 K, in the frequency range of the electron-molecular vibration-activated ν_3 mode, for (a) the more conductive direction (**E**||**b-a**) and (b) the perpendicular to the more conductive direction (**E**||**b**+**a**). Insets in panels (a) and (b) display a close-up view of the temperature dependence of the ν_{3H} mode at 1446 cm^{-1} mode that appears in both spectra below 30 K.

Table IV. Experimental Raman and infrared (IR) frequencies (cm^{-1}) of the ν_3 mode components in β'-(BEDT-TTF)$_2$CF$_3$CF$_2$SO$_3$ at temperatures $T = 300$ K and 10 K.

Raman		IR		IR	
$\parallel (b+a)$		$E \parallel (b-a)$		$E \parallel (b+a)$	
300 K	10 K	300 K	10 K	300 K	10 K
1469	1472				
			1446		1447
				1374	1383
		$\sim$ 1327	$\sim$ 1333		

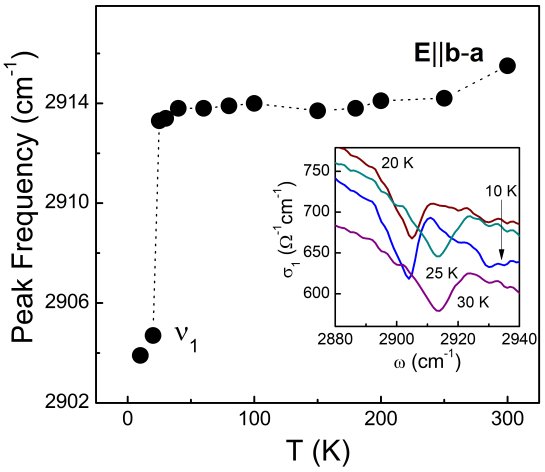

Figure 7. The ν_1 vibrational BEDT-TTF mode observed in the more conductive **E**||**b-a** direction observed in optical conductivity spectra of β'-(BEDT-TTF)$_2$CF$_3$CF$_2$SO$_3$, inset: optical conductivity spectra at 10, 20, 25 and 30 K in this frequency range.

ble IV). Unfortunately, no crystal data are available at low T to verify a possible symmetry lowering in β'-(BEDT-TTF)$_2$CF$_3$CF$_2$SO$_3$ at the charge order transition as suggested by the Raman results. Nevertheless, the softening and intensity enhancement of several vibrational modes observed in the optical conductivity spectra (see the ν_3 mode components in Fig. 5(c) and in Supplemental Material,[39] Fig. S10) and temperature dependence of the mid-infrared electronic excitations below 25 K (Fig. 4) are also consistent with a structural modification.

This low-temperature lattice effect in the BEDT-TTF donor layer most probably involves the significant change regarding interactions between ethylene end groups of the donor molecule and the $CF_3CF_2SO_3^-$ anions, both involved in providing a connection between neighbouring donor layers through the anion layer. In fact, when lowering the temperature between 25 and 20 K we observe a striking 10 cm^{-1} redshift of ν_1, the C-H symmetric stretching mode of the BEDT-TTF ethylene groups, indicating a sudden C-H bond lengthening (Fig. 7). Other vibrational modifications related with the ordering of the terminal ethylene groups that is characteristic for BEDT-TTF-based organic charge transfer salts is shown in Supplemental Material [39] (see, also, references [40, 41] therein).

DISCUSSION

The results of the presented Raman study provide a strong evidence for a sharp charge order transition in β'-(BEDT-TTF)$_2$CF$_3$CF$_2$SO$_3$ at $T \approx 20$ K, with $2\delta\rho \approx 0.1e$. This finding is consistent with both the crystal structure data and electronic band structure calculations that suggest a possibility of interlayer charge disproportionation due to the presence of two nonequivalent donor layers in the unit cell. The Dimer Mott response observed in the optical conductivity spectra is also in agreement

with such a scenario.[54] An interlayer charge disproportionation resulting in the appearance of charge-rich and charge-poor layers in the crystal structure, is rather unique among BEDT-TTF salts. In particular, it suggests a possibility of charge transfer between neighbouring donor layers. The interlayer charge disproportionation is essentially different than the intradimer charge disproportionation suggested for β'-(BEDT-TTF)$_2$ICl$_2$ based on a dielectric study,[57] and recently investigated using Raman spectra measured under an electric field.[51]

In β'-(BEDT-TTF)$_2$CF$_3$CF$_2$SO$_3$, a significant redshift of ν_1 below 25 K (Fig. 7(b)) implies, that both a low-temperature lattice distortion and charge order are strongly related with distinct structural changes involving counterions and short contacts of the hydrogen-bonding character that are present between BEDT-TTF molecule and $CF_3CF_2SO_3^-$ anion. A specific pattern of such an interaction is known to participate in the disorder-driven localization in case of β''-(BEDT-TTF)$_2$SF$_5$CHFCF$_2$SO$_3$.[58] The cation-anion interactions are also suggested to induce or stabilize charge-ordered state in some other dimerized BEDT-TTF conductors.[59, 60] On the other hand, charge disproportionation present in the material can cause shifts of anions due to the modified electrostatic interactions.[11] Therefore a question arises, if charge ordering and symmetry lowering in β'-(BEDT-TTF)$_2$CF$_3$CF$_2$SO$_3$ is due or related with the cation-anion interactions. As we already discussed, the anions remain disordered both at room temperature and at 100 K. On the other hand, the low-temperature redshift of the ν_1 mode we observe is probably due to the shortening of the hydrogen bond between the donor and anion molecules. Such an effect suggests that anions become ordered below 25 K, resulting in the more rigid lattice of the lower symmetry. Having in mind that the interlayer charge disproportionation in β'-(BEDT-TTF)$_2$CF$_3$CF$_2$SO$_3$ is structurally allowed already at room temperature, we suggest that the modification in the cation-anion interaction pattern is rather a result of the appearance of charge order at low temperature, than a driving force.

CONCLUSIONS

The β'-(BEDT-TTF)$_2$CF$_3$CF$_2$SO$_3$ organic conductor has been crystallized and characterized by X-ray diffraction measurements, optical experiments, and electronic band structure calculations. Based on optical conductivity measurements we identify the Mott nature of this system. The Raman spectra show that a (possibly interlayer) charge-ordered state develops in this material below 25 K. In the same temperature range in the infrared spectra we observe significant signatures of lattice distortion. We find that the transition has a strong influence on the interactions between the conducting cation layer and the anion layer. The ordering of the BEDT-TTF ethylene groups below 150 K is detected both by the structural measurements and by the infrared study.

Further structural measurements are needed to confirm the low-temperature lattice distortion. At the same time, a magnetic study would be essential to examine the possibility of the interplay between charge, lattice and spin degrees of freedom in β'-(BEDT-TTF)$_2$CF$_3$CF$_2$SO$_3$. This remains a subject of future studies.

ACKNOWLEDGEMENTS

JAS acknowledges support from the Independent Research/Development program while serving at the National Science Foundation. Work supported by UChicago Argonne, LLC, Operator of Argonne National Laboratory ("Argonne"). Argonne, a US Department of Energy Office of Science laboratory, is operated under Contract No. DE-AC02-06CH11357. HOJ and RV acknowledge funding from the Deutsche Forschungsgemeinschaft within collaborative research center SFB/TR 49. Authors thank Janice L. Musfeldt for help in room temperature FIR and NIR reflectance measurements, and numerous discussions. We also thank R. Wojciechowski for help in interpretation of Raman spectra. We thank Brian H. Ward for his contributions to the synthetic effort at Argonne.

Supplemental Information

Crystallographic data for the β'-(BEDT-TTF)$_2$CF$_3$CF$_2$SO$_3$ structure at 100 and 300 K has been deposited in CIF format with the Cambridge Crystallographic Data Centre witth CCDC numbers 1428646 and 1428647, respectively. Copies of this data can be obtained free of charge from https://summary.ccdc.cam.ac.uk/structure-summary-form or by application to CCDC, 12 Union Road, Cambridge CB2 1EZ, UK (fax: (44) 1223 336-033; e-mail: data_request@ccdc. cam.ac.uk).

[1] B. J. Powell, R. H. McKenzie, Quantum frustration in organic Mott insulators: from spin liquids to unconventional superconductors, Rep. Prog. Phys. **74**, 056501 (2011).

[2] H. Mori, Materials Viewpoint of Organic Superconductors, J. Phys. Soc. Jpn. **75**, 051003 (2006).

[3] J. M. Williams, J. R. Ferraro, R. J. Thorn, K. D. Carlson, U. Geiser, H. H. Wang, A. M. Kini, M. H. Whangbo, Organic Superconductors (Including Fullerenes); Prentice Hall: Englewood Cliffs, New Jersey, 1992.

[4] N. Toyota, M. Lang, J. Müller, Low-Dimensional Molecular Metals; Springer-Verlag: Berlin, 2007.

[5] H. C. Kandpal, I. Opahle, Y.-Z. Zhang, H. O. Jeschke, R. Valenti, Revision of Model Parameters for κ-Type Charge

Transfer Salts: An Ab Initio Study, Phys. Rev. Lett. **103**, 067004 (2009).

[6] M. Dressel, N. Drichko, Optical Properties of Two-Dimensional Organic Conductors: Signatures of Charge Ordering and Correlation Effects, Chem. Rev. **104**, 5689 (2004).

[7] H. Seo, C. Hotta, and H. Fukuyama, Toward Systematic Understanding of Diversity of Electronic Properties in Low-Dimensional Molecular Solids, Chem. Rev. **104**, 5005 (2004).

[8] C. Hotta, Theories on Frustrated Electrons in Two-Dimensional Organic Solids, Crystals **2**, 1155 (2012).

[9] R. Kaneko, L. F. Tocchio, R. Valentí, F. Becca, Charge orders in organic charge-transfer salts, New J. Phys. **19**, 103033 (2017).

[10] Yi Zhou, Kazushi Kanoda, and Tai-Kai Ng, Quantum spin liquid states, Rev. Mod. Phys. **89**, 025003 (2017).

[11] E. Gati, J. K. H. Fischer, P. Lunkenheimer, D. Zielke, S. Köhler, F. Kolb, H.-A. Krug von Nidda, S. M. Winter, H. Schubert, J. A. Schlueter, H. O. Jeschke, R. Valentí, and M. Lang, Evidence for Electronically Driven Ferroelectricity in a Strongly Correlated Dimerized BEDT-TTF Molecular Conductor, Phys. Rev. Lett. **120**, 247601 (2018).

[12] M. Matsuura, T. Sasaki, S. Iguchi, E. Gati, J. Müller, O. Stockert, A. Piovano, M. Böhm, J. T. Park, S. Biswas, S. M. Winter, R. Valentí, A. Nakao, M. Lang, Lattice Dynamics Coupled to Charge and Spin Degrees of Freedom in the Molecular Dimer-Mott Insulator $\kappa-(\mathrm{BEDT-TTF})_2\mathrm{Cu[N(CN)_2]Cl}$, Phys. Rev. Lett. **123**, 027601 (2019).

[13] J. A. Schlueter, B. H. Ward, U. Geiser, H. H. Wang, A. M. Kini, J. P. Parakka, E. Morales, H.-J. Koo, M.-H. Whangbo, R. W. Winter, J. Mohtasham, and G. L. Gard, Crystal structure, physical properties and electronic structure of a new organic conductor β''-$(\mathrm{BEDT\text{-}TTF})_2\mathrm{SF_5CHFCF_2SO_3}$, J. Mater. Chem. **11**, 2008 (2001).

[14] B. H. Ward, J. A. Schlueter, U. Geiser, H. H. Wang, E. Morales, J. P. Parakka, S. Y. Thomas, J. M. Williams, P. G. Nixon, R. W. Winter, G. L. Gard, H.-J. Koo, and M.-H. Whangbo, Comparison of the Crystal and Electronic Structures of Three 2:1 Salts of the Organic Donor Molecule BEDT-TTF with Pentafluorothiomethylsulfonate Anions $\mathrm{SF_5CH_2SO_3^-}$, $\mathrm{SF_5CHFSO_3^-}$, and $\mathrm{SF_5CF_2SO_3^-}$, Chem. Mater. **12**, 343 (2000).

[15] U. Geiser, J. A. Schlueter, H. H. Wang, A. M. Kini, J. M. Williams, P. P. Sche, H. I. Zakowicz, M. L. VanZile, J. D. Dudek, P. G. Nixon, R. W. Winter, G. L. Gard, J. Ren, M.-H. Whangbo, Superconductivity at 5.2 K in an Electron Donor Radical Salt of Bis(ethylenedithio)tetrathiafulvalene (BEDT-TTF) with the Novel Polyfluorinated Organic Anion $\mathrm{SF_5CH_2CF_2SO_3^-}$, J. Am. Chem. Soc. **118**, 9996 (1996).

[16] S. Kaiser, M. Dressel, Y. Sun, A. Greco, J. A. Schlueter, G. L. Gard, N. Drichko, Bandwidth Tuning Triggers Interplay of Charge Order and Superconductivity in Two-Dimensional Organic Materials, Phys. Rev. Lett. **105**, 206402 (2010).

[17] A. Pustogow, Y. Saito, A. Rohwer, J. A. Schlueter, and M. Dressel, Coexistence of charge order and superconductivity in β''-$(\mathrm{BEDT\text{-}TTF})_2\mathrm{SF_5CH_2CF_2SO_3}$, Phys. Rev. B **99**, 140509(R) (2019).

[18] J. Merino, and R. H. McKenzie, Superconductivity Mediated by Charge Fluctuations in Layered Molecular Crystals, Phys. Rev. Lett. **87**, 237002 (2001).

[19] B. H. Ward, I. B. Rutel, J. S. Brooks, J. A. Schlueter, R. W. Winter, and G. L. Gard, Millimeter-Wave Spectroscopy of the Organic Spin-Peierls System β'-$(\mathrm{ET})_2\mathrm{SF_5CF_2SO_3}$, J. Phys. Chem. B **105**, 1750 (2001).

[20] J. M. Pigos, B. R. Jones, Z.-T. Zhu, J. L. Musfeldt, C. C. Homes, H.-J. Koo, M.-H. Whangbo, J. A. Schlueter, B. H. Ward, H. H. Wang, U. Geiser, J. Mohtasham, R. W. Winter, and G. L. Gard, Infrared and Optical Properties of β'-$(\mathrm{ET})_2\mathrm{SF_5CF_2SO_3}$: Evidence for a 45 K Spin-Peierls Transition, Chem. Mater. **13**, 1326 (2001).

[21] I. B. Rutel, S. A. Zvyagin, J. S. Brooks, J. Krzystek, P. Kuhns, A. P. Reyes, E. Jobiliong, B. H. Ward, J. A. Schlueter, R. W. Winter, and G. L. Gard, High-field magnetic resonant properties of β'-$(\mathrm{ET})_2\mathrm{SF_5CF_2SO_3}$, Phys. Rev. B **67**, 214417 (2003).

[22] J. A. Schlueter, B. H. Ward, U. Geiser, J. Mohtasham, R. W. Winter, and G. L. Gard, Chemical modification of the superconducting β'-$(\mathrm{ET})_2\mathrm{SF_5CH_2CF_2SO_3}$ structure through use of $\mathrm{CF_3}C\mathit{RR''}\mathrm{SO_3^-}$ Anions, Mol. Cryst. Liq. Cryst. **380**, 129 (2002).

[23] T. K. Hansen, J. Becher, T. Jørgensen, K. S. Varma, R. Khedekar, M. P. Cava, 4,5Dibenzoyl1,3Dithiole2Thione: Benzenecarbothioic acid, S,S'(2thioxo1,3dithiole4,5diyl) ester, Org. Synth. **73**, 270 (1995).

[24] K. S. Varma, A. Bury, N. J. Harris, A. E. Underhill, Improved synthesis of bis (ethylenedithio) tetrathiafulvalene (BEDT-TTF): π-Donor for synthetic metals, Synthesis **1987**, 837 (1987).

[25] G. A. Olah, T. Weber, D. R. Bellew, O. Farooq, One-Pot Preparation of Pentafluoroethanesulfonic (Pentflic) Acid by the Organolithium Pathway, Synthesis **1989**, 463 (1989).

[26] T. J. Emge, H. H. Wang, M. A. Beno, J. M. Williams, M.-H. Whangbo, M. Evain, Effect of anion ordering on the H-anion interactions and band electronic structure of $(\mathrm{TMTSF})_2\mathrm{BF_4}$ at 20 K, J. Am. Chem. Soc. **108**, 8215 (1986).

[27] D. A. Stephens, A. E. Rehan, S. J. Compton, R. A. Barkhau, J. M. Williams, Tetrabutylammonium perchlorate and bis($4,4',5,5'$-tetramethyl-$2,2'$-bi-1,3-diselenolylidene) radical ion (1+) perchlorate, Inorg. Synth. **24**, 135 (1986).

[28] G. M. Sheldrick, SADABS, Version 2.03a, Bruker AXS, Inc., Madison, WI, USA, 2001.

[29] G. M. Sheldrick, SHELXTL, Version 6.12, Bruker AXS Inc., Madison, WI, USA, 2001.

[30] K. Koepernik and H. Eschrig, Full-potential nonorthogonal local-orbital minimum-basis band-structure scheme, Phys. Rev. B **59**, 1743 (1999); http://www.FPLO.de

[31] J. P. Perdew, K. Burke and M. Ernzerhof, Generalized Gradient Approximation Made Simple, Phys. Rev. Lett. **77**, 3865 (1996).

[32] H. Eschrig, K. Koepernik, Tight-binding models for the iron-based superconductors, Phys. Rev. B **80**, 104503 (2009).

[33] F. Wooten, Optical Properties of Solids, Academic Press, New York, **1972**.

[34] A. Graja, I. Olejniczak, B. Barszcz, and J. A. Schlueter, Vibrational spectra of two BEDT-TTF-based organic conductors: charge order, Cent. Eur. J. Phys. **7**, 663 (2009). This conference paper reports conductivity spectra of β'-$(\mathrm{BEDT\text{-}TTF})_2\mathrm{CF_3CF_2SO_3}$ at 300 K and 10 K,

together with preliminary Raman data measured in a limited temperature range that is replaced with more accurate results in the current paper.

[35] T. J. Emge, H. H. Wang, P. C. W. Leung, P. R. Rust, J. D. Cook, P. L. Jackson, K. D. Carlson, J. M. Williams, M.-H. Whangbo, E. L. Venturini, J. E. Schirber, L. J. Azevedo, and J. R. Ferraro, New Cation-Anion Interaction Motifs, Electronic Band Structure, and Electrical Behavior in β-$(ET)_2X$ Salts ($X = IC1_2^-$ and $BrICl^-$), J. Am. Chem. Soc. **108**, 695 (1986).

[36] T. J. Emge, H. H. Wang, M. K. Bowman, C. M. Pipan, K. D. Carlson, M. A. Beno, L. N. Hall, B. A. Anderson, J. M. Williams, and M.-H. Whangbo, The Anisotropy of Intermolecular Interactions, Band Electronic Structure, and Electrical Properties of β-$(ET)_2AuCl_2$, J. Am. Chem. Soc. **109**, 2016 (1987).

[37] T. Mori, Structural Genealogy of BEDT-TTF-Based Organic Conductors I. Parallel Molecules: β and β'' Phases, Bull. Chem. Soc. Jpn. **71**, 2509 (1998).

[38] R. Kato, Conducting Metal Dithiolene Complexes: Structural and Electronic Properties, Chem. Rev. **104**, 5319 (2004).

[39] See Supplemental Material at [URL] for additional crystal structures including thermal ellipsoid plots, electronic bandstructures and vibrational effects related with the lattice distortion, other than shown in the main text.

[40] P. C. W. Leung, T. J. Emge, M. A. Beno, H. H. Wang, J. M. Williams, V. Petricek, P. Coppens, Novel structural modulation in the ambient-pressure sulfur-based organic superconductor β-$(BEDT\text{-}TTF)_2I_3$: origin and effects on its electrical conductivity, J. Am. Chem. Soc. **107**, 6184 (1985).

[41] D. Guterding, R. Valentí, and H. O. Jeschke, Influence of molecular conformations on the electronic structure of organic charge transfer salts, Phys. Rev. B **92**, 081109(R) (2015), and references therein.

[42] J. Ferber, K. Foyevtsova, H. O. Jeschke, and R. Valentí, Unveiling the microscopic nature of correlated organic conductors: The case of κ-$(ET)_2Cu[N(CN)_2]Br_xCl_{1-x}$, Phys. Rev. B **89**, 205106 (2014).

[43] M. J. Rice, Organic Linear Conductors as Systems for the Study of Electron-Phonon Interactions in the Organic Solid State, Phys. Rev. Lett. **37**, 36 (1976).

[44] M. J. Rice, N. O. Lipari, and S. Strässler, Dimerized Organic Linear-Chain Conductors and the Unambiguous Experimental Determination of Electron-Molecular-Vibration Coupling Constants, Phys. Rev. Lett. **39**, 1359 (1977).

[45] D. Faltermeier, J. Barz, M. Dumm, M. Dressel, N. Drichko, B. Petrov, V. Semkin, R. Vlasova, C. Mezière, and P. Batail, Bandwidth-controlled Mott transition in κ-$(BEDT\text{-}TTF)_2Cu[N(CN)_2]Br_xCl_{1-x}$: Optical studies of localized charge excitations, Phys. Rev. B **76**, 165113 (2007).

[46] K. Hashimoto, R. Kobayashi, H. Okamura, H. Taniguchi, Y. Ikemoto, T. Moriwaki, S. Iguchi, M. Naka, S. Ishihara, and T. Sasaki, Emergence of charge degrees of freedom under high pressure in the organic dimer-Mott insulator β'-$(BEDT\text{-}TTF)_2ICl_2$, Phys. Rev. B **92**, 085149 (2015).

[47] T. Yamamoto, M. Uruichi, K. Yamamoto, K. Yakushi, A. Kawamoto, and H. Taniguchi, Examination of the Charge-Sensitive Vibrational Modes in Bis(ethylenedithio)tetrathiafulvalene, J. Phys. Chem. B **109**, 15226 (2005).

[48] K. Yamamoto, K. Yakushi, K. Miyagawa, K. Kanoda, and A. Kawamoto, Charge ordering in θ-$(BEDT\text{-}TTF)_2RbZn(SCN)_4$ studied by vibrational spectroscopy, Phys. Rev. B **65**, 085110 (2002).

[49] As a rule, the infrared-active ν_{27} mode appears in the infrared spectra in the polarization perpendicular to the conducting plane. In case of β'-$(BEDT\text{-}TTF)_2CF_3CF_2SO_3$ such a measurement was not possible.

[50] R. Wojciechowski, unpublished results.

[51] Y. Hattori, S. Iguchi, T. Sasaki, S. Iwai, H. Taniguchi, and H. Kishida, Electric-field-induced intradimer charge disproportionation in the dimer-Mott insulator β'-$(BEDT\text{-}TTF)_2ICl_2$, Phys. Rev. B **95**, 085149 (2017).

[52] A. Girlando, M. Masino, S. Kaiser, Y. Sun, N. Drichko, M. Dressel, and H. Mori, Spectroscopic characterization of charge order fluctuations in BEDT-TTF metals and superconductors, Phys. Status Solidi B **249**, 953-956 (2012).

[53] A. Girlando, M. Masino, J. A. Schlueter, N. Drichko, S. Kaiser, and M. Dressel, Spectroscopic characterization of charge order fluctuations in BEDT-TTF metals and superconductors, Phys. Rev. B **89**, 174503 (2014).

[54] A. Pustogow, K. Treptow, A. Rohwer, Y. Saito, M. Sanz Alonso, A. Löhle, J. A. Schlueter, and M. Dressel, Charge order in β''-phase BEDT-TTF salts, Phys. Rev. B **99**, 155144 (2019).

[55] T. Yamamoto, H. M. Yamamoto, R. Kato, M. Uruichi, K. Yakushi, H. Akutsu, A. Sato-Akutsu, A. Kawamoto, S. S. Turner, and P. Day, Inhomogeneous site charges at the boundary between the insulating, superconducting, and metallic phases of β''-type bis-ethylenedithiotetrathiafulvalene molecular charge-transfer salts, Phys. Rev. B **77**, 205120 (2008).

[56] K. Suzuki, K.Yamamoto, and K. Yakushi, Charge-ordering transition in orthorhombic and monoclinic single-crystals of θ-$(BEDT\text{-}TTF)_2TlZn(SCN)_4$ studied by vibrational spectroscopy, Phys. Rev. B **69**, 085114 (2004).

[57] S. Iguchi, S. Sasaki, N. Yoneyama, H. Taniguchi, T. Nishizaki, and T. Sasaki, Relaxor ferroelectricity induced by electron correlations in a molecular dimer Mott insulator, Phys. Rev. B **87**, 075107 (2013).

[58] B. R. Jones, I. Olejniczak, J. Dong, J. M. Pigos, Z. T. Zhu, A. D. Garlach, J. L. Musfeldt, H.-J. Koo, M.-H. Whangbo, J. A. Schlueter, B. H. Ward, E. Morales, A. M. Kini, R. W. Winter, J. Mohtasham, and G. L. Gard, Optical Spectra and Electronic Band Structure Calculations of β''-$(ET)_2SF_5RSO_3$ ($R = CH_2CF_2$, $CHFCF_2$, and CHF): Changing Electronic Properties by Chemical Tuning of the Counterion, Chem. Mater. **12**, 2490 (2000).

[59] J.-P. Pouget, P. Alemany, and E. Canadell, Donoranion interactions in quarter-filled low-dimensional organic conductors, Mater. Horiz. **5**, 590 (2018).

[60] M. Sawada, S. Fukuoka, and A. Kawamoto, Coupling of molecular motion and electronic state in the organic molecular dimer Mott insulator β'-$(BEDT\text{-}TTF)_2ICl_2$, Phys. Rev. B **97**, 045136 (2018).